View metadata, citation and similar papers at core.ac.uk
brought to you by CORE

東北大学機関リポジトリ
TOUR
Tohoku University Repository

Bias-voltage dependence of magnetoresistance in magnetic tunnel junctions grown on Al2O3 (0001) substrates

著者	安藤　康夫
journal or publication title	Applied Physics Letters
volume	86
page range	102506-1-102506-3
year	2005-05
URL	http://hdl.handle.net/10097/34660

HTML ABSTRACT + LINKS

Bias-voltage dependence of magnetoresistance in magnetic tunnel junctions grown on Al_2O_3 (0001) substrates

Sung-Jin Ahn,[a] Takeharu Kato, Hitoshi Kubota, Yasuo Ando, and Terunobu Miyazaki
Department of Applied Physics, Graduate School of Engineering, Tohoku University, Aoba-yama 05, Sendai 980-8579, Japan

(Received 9 July 2004; accepted 17 January 2005; published online 4 March 2005)

Magnetic tunnel junctions with the structure of Al_2O_3 (0001)/Pt (111) 20 nm/$Ni_{80}Fe_{20}$ (111) 50 nm/Al 1.6 nm–O/$Co_{75}Fe_{25}$ 4 nm/$Ir_{22}Mn_{78}$ 10 nm/$Ni_{80}Fe_{20}$ 30 nm were fabricated using UHV sputtering and photolithography process. As the annealing temperature increased up to 250 °C, tunnel magnetoresistance (TMR) ratio at 1 mV bias increased from 28% to 43% for $t_{ox}=180$ s plasma oxidation and the $V_{\pm 1/2}$, at which the zero bias TMR value is halved, is +640 mV and −650 mV for positive and negative bias voltages, respectively. The bias-voltage dependence of TMR could be explained in terms of the relationship with $V_{\pm 1/2}$ and the interface of the ferromagnetic electrode and the Al–O insulating layer. $V_{+1/2}$, which reflects the bottom ferromagnetic electrode-barrier interface state, changes with plasma oxidation time, while $V_{-1/2}$, which corresponds to top ferromagnetic electrode-barrier interface, hardly changes. © *2005 American Institute of Physics*. [DOI: 10.1063/1.1870104]

Magnetic tunnel junctions (MTJs) have been extensively investigated due to their fertile physics and potential applications since the discovery of a large tunnel magnetoresistance (TMR) ratio at room temperature.[1,2] One of the main problems in application of MTJs is the dramatic decrease of TMR ratio with applied bias voltage.[2] It is reported that the decrease of TMR ratio with bias voltage results from voltage-dependent density of state at the Fermi level,[3,4] electronic structure of ferromagnetic (FM) electrode, and magnon excitation at the metal-barrier interface.[5] Experimental results show, however, that the oxidation condition of the tunnel junctions also influences its bias-voltage dependence. Zhang and White[6] explained successfully the voltage and temperature dependence of TMR through two-step tunneling via defect states such as magnetic impurities and metal particles. Conclusively, the bias-voltage dependence of TMR is strongly related not only to the quality of the interfaces and barrier but also to the FM electrode.

It is reported that metallic Al layer grows epitaxially on NiFe (111) layer in spite of the large lattice mismatch (~12%),[7] which suggests that metallic Al layer can be grown on NiFe (111) without any high-angle grain boundaries so that a relatively uniform Al–O insulating layer and clean FM layer-insulator interfaces can be formed compared to the polycrystalline MTJs. Therefore, in this work, we aim at improving the bias-voltage dependence of TMR through epitaxially grown bottom FM electrode and uniform tunnel barrier resulting from oxidation of the metallic Al layer deposited on the epitaxially grown electrode. Furthermore, we discuss the changes of $V_{\pm 1/2}$, at which the zero bias TMR value is halved, with plasma oxidation time at different annealing temperatures in terms of interface between FM electrode and Al–O insulating layer, which has not been reported systematically.

MTJs were prepared by magnetron sputtering on Al_2O_3 (0001) substrates. The stacking structure of multilayers was Al_2O_3 (0001)/Pt (111) 20 nm/$Ni_{80}Fe_{20}$ (111) 50 nm/Al 1.6 nm–O/$Co_{75}Fe_{25}$ 4 nm/$Ir_{22}Mn_{78}$ 10 nm /$Ni_{80}Fe_{20}$ 30 nm. Prior to deposition, Al_2O_3 (0001) substrates were heated up to 850 °C for 30 min to rearrange the surface structure and the Pt buffer layer was deposited at 300 °C. After cooling down, the other layers were deposited at room temperature (RT). All the deposition processes were done at a base pressure of about 1×10^{-6} Pa without breaking vacuum. In order to obtain epitaxially grown films, the buffer layer (Pt) and the bottom FM electrode ($Ni_{80}Fe_{20}$) were sputtered at the slow rate of 0.06 and 0.03 nm/s, respectively. After sputtering of ultrathin Al layers, the surface was oxidized by inductively coupled plasma in a mixed atmosphere of 0.25 Pa Ar and 0.75 Pa O_2. Plasma oxidation time was changed from 120 to 300 s. Tunnel junctions were fabricated using microfabrication process combined with Ar ion-beam etching and CHF_3 reactive ion etching. Crystallographic properties were exam-

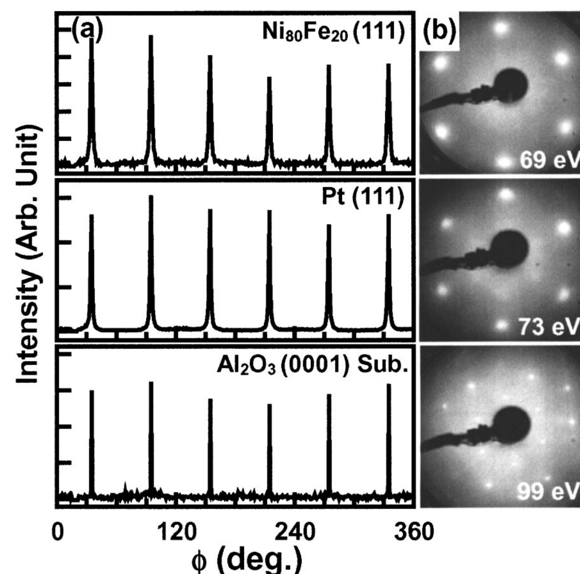

FIG. 1. (a) The ϕ scan and (b) LEED pattern of Al_2O_3 (0001) /Pt (111) 20 nm/$Ni_{80}Fe_{20}$ (111) 20 nm.

[a]Author to whom correspondence should be addressed; electronic mail: sjahn@mlab.apph.tohoku.ac.jp

 © 2005 American Institute of Physics
Downloaded 11 Jun 2008 to 130.34.135.158. Redistribution subject to AIP license or copyright; see http://apl.aip.org/apl/copyright.jsp

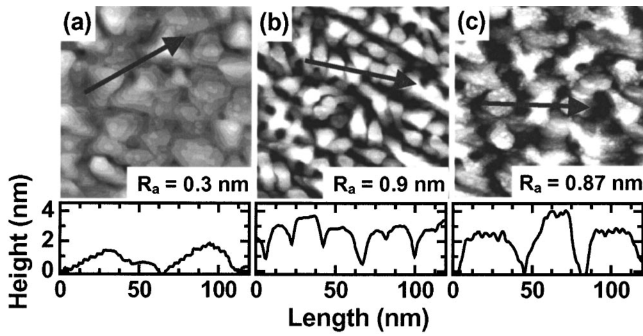

FIG. 2. STM images of (a) Pt, (b) $Ni_{80}Fe_{20}$, and (c) Al surfaces and cross section profiles of the Al_2O_3 (0001)/Pt (111) 20 nm/$Ni_{80}Fe_{20}$ (111) 50 nm/Al 1.6 nm. The scan area is 200 nm × 200 nm.

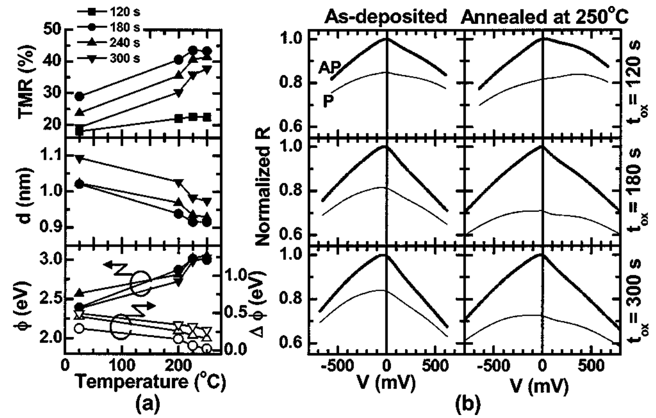

FIG. 3. (a) The changes of TMR ratio, barrier width, average barrier height, and barrier height symmetry with annealing temperature. (b) The normalized resistance-bias voltage curve before and after annealing for three junctions with different oxidation time.

ined using x-ray diffraction (XRD) and low energy electron diffraction (LEED). Scanning tunnel microscopy (STM) images were examined without breaking vacuum in order to investigate the growth mode, surface morphology, and roughness. TMR loops and current-voltage (*I-V*) curves were measured at RT by a four-probe method. The bias-voltage dependence of TMR was obtained from *I-V* curves at parallel and antiparallel magnetization configurations between the top and bottom FM electrodes.

The rocking curves measured for the Pt (111) and the $Ni_{80}Fe_{20}$ (111) peaks showed the full width at half maximum of 0.04° and 0.4°, respectively. Figure 1 shows x-ray diffraction ϕ scan (a) and LEED patterns (b) of the Al_2O_3 (0001)/Pt (111) 20 nm/$Ni_{80}Fe_{20}$ (111) 20 nm. From the peak positions of Pt (111) and $Ni_{80}Fe_{20}$ (111) with respect to those of Al_2O_3 (0001) and their LEED patterns, it is confirmed that Pt (111) and NiFe (111) [fcc structure] grow epitaxially on Al_2O_3 (0001) [corundrum structure]. However, the sixfold symmetry from Pt (111) and $Ni_{80}Fe_{20}$ (111) observed from the x-ray diffraction ϕ scans [Fig. 1(a)] indicates twin epitaxy with some grains rotated by 180° about the [111] pole with respect to others.[8]

Figure 2 shows STM images and their cross section profiles of (a) Pt, (b) $Ni_{80}Fe_{20}$, and (c) Al with structure of the Al_2O_3 (0001) /Pt (111) 20 nm/$Ni_{80}Fe_{20}$ (111) 50 nm/Al 1.6 nm without breaking vacuum. As can be seen in Fig. 2(a), Pt (111) grew in layer-by-layer mode on Al_2O_3 (0001) substrate and its surface roughness is 0.3 nm. On the other hand, the roughness of $Ni_{80}Fe_{20}$ (111) deposited on Pt (111) increased to 0.9 nm [Fig. 2(b)]. This abrupt increase is probably due to the large difference of lattice parameter (a_{NiFe} $=0.355$ nm, $a_{Pt}=0.392$ nm). The roughness of Al 1.6 nm, which is shown in Fig. 2(c), is almost the same as that of $Ni_{80}Fe_{20}$ (111). It is noted that the Al layer is grown densely on $Ni_{80}Fe_{20}$ (111) and its morphology is similar to that of $Ni_{80}Fe_{20}$ (111).

The changes of TMR ratio, barrier width (d), average barrier height (Φ), and barrier height symmetry ($\Delta\phi$) with oxidation time at different annealing temperatures are shown in Fig. 3(a). For a sample oxidized for $t_{ox}=120$ s, the increase of TMR ratio was small and average barrier height and barrier width could not be deduced because its *I-V* curve was not able to be fitted by Brinkman's equation, which suggests that metallic Al remains at interface between the bottom FM electrode and the Al–O insulating layer before and after annealing. As the annealing temperature increased up to 250 °C for 1 h [Fig. 3(a)], the TMR ratio increased from 28% to 43% for $t_{ox}=180$ s oxidation time. An average barrier height (Φ) increased from 2.4 up to about 3 eV and the difference $\Delta\phi$ between bottom barrier height (ϕ_1) and top barrier height (ϕ_2) decreased, which means that the barrier shape becomes near to a rectangular potential barrier after annealing. The effective barrier thickness decreased from 1.0 to 0.9 nm, which suggested homogeneity of Al–O layer and sharpening of the FM/I interfaces due to the annealing. For samples oxidized for $t_{ox}=240$ and 300 s, smaller TMR ratios and larger $\Delta\phi$ were observed compared to those of a sample for $t_{ox}=180$ s due to the oxidized FM which might cause a decrease in spin polarization of the bottom FM electrode and barrier height at interface between the bottom FM electrode and Al–O insulating layer.

The normalized resistance-voltage curves with oxidation time are described in Fig. 3(b). The left column and right one represent curves of before and after annealing, respectively. In our experiments, the direction of current is from the bottom electrode to the top electrode when the positive bias voltage is applied. Therefore, it is worth noting that, considering the report of Brinkman, Dynes, Rowell,[9] the positive bias region reflects bottom barrier height (ϕ_1) while the negative bias region reflects top barrier height (ϕ_2). The oxidation condition can be estimated by the shape of conductance or resistance curve[10] as well as by the TMR ratio and barrier height symmetry $\Delta\phi$; the strong plasma oxidation can produce magnetic oxide at the interface between the bottom FM layer and Al–O layer, so that bottom barrier height (ϕ_1) decreases. Similarly, when it is under oxidized and the Al layer is not fully oxidized, the right side of resistance is

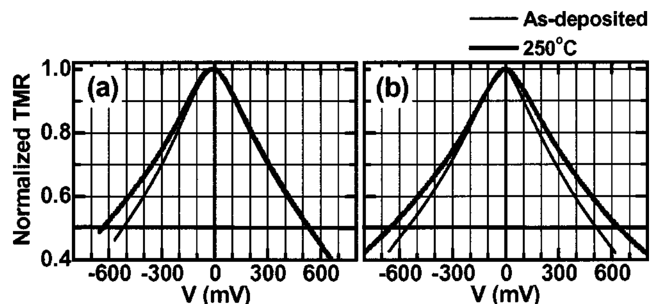

FIG. 4. The normalized TMR ratio vs dc bias-voltage curves measured at RT with annealing for (a) $t_{ox}=120$ s and (b) $t_{ox}=180$ s.

Downloaded 11 Jun 2008 to 130.34.135.158. Redistribution subject to AIP license or copyright; see http://apl.aip.org/apl/copyright.jsp

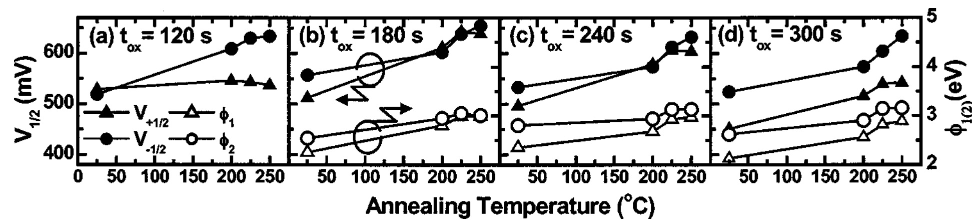

FIG. 5. The changes of $V_{\pm 1/2}$ and barrier height $\phi_{1(2)}$ with annealing temperature for four junctions with different oxidation time.

higher. When over oxidized, the right side is lower. As can be seen in the left column of Fig. 3(b), the right side of resistance curve is higher than the corresponding left side for $t_{ox}=120$ s while the right side is lower for $t_{ox}=300$ s. After annealing for the sample oxidized for $t_{ox}=300$ s, asymmetry of resistance curve is reduced, which also means that the annealing improves the quality of barrier and interface. Therefore, in this experiment, we can regard $t_{ox}=180$ s as the proper oxidation time, for which the normalized *R-V* curve is the most symmetric.

Figure 4 represents the normalized TMR ratio vs dc bias-voltage curves measured at RT with annealing for $t_{ox}=120$ s and $t_{ox}=180$ s. In general, TMR decay can be evaluated with the voltage $V_{\pm 1/2}$, at which the zero bias TMR value is halved. In particular, the changes of $V_{\pm 1/2}$ with annealing for $t_{ox}=120$ s were unique; $V_{-1/2}$ increases while $V_{\pm 1/2}$ does not change due to under oxidation. For proper oxidation time $t_{ox}=180$ s [Fig. 4(b)], the $V_{\pm 1/2}$ was $+640$ mV and -650 mV for positive and negative bias voltages, respectively, when annealed at 250 °C. These values of $V_{\pm 1/2}$ were enhanced results compared to those of polycrystalline MTJs which have been reported.[11–14]

Similar to ϕ_1 and ϕ_2, we could assume that $V_{+1/2}$ and $V_{-1/2}$ also reflect the bottom FM layer-insulator interface (*bottom interface*) and the top FM layer-insulator interface (*top interface*), respectively. Figure 5 shows the changes of $V_{\pm 1/2}$ and barrier height $\phi_{1(2)}$ as a function of annealing temperature for various plasma oxidation conditions. From Fig. 5(a), it can be seen that $V_{+1/2}$ hardly changed while $V_{-1/2}$ increased with increasing annealing temperature when under oxidized ($t_{ox}=120$ s). This may suggest that in the under-oxidized barrier, due to oxygen deficiency, oxygen cannot diffuse to the *bottom interface* when annealed, leaving metallic Al residue at the *bottom interface* even after annealing. Therefore, $V_{+1/2}$, which is related to the quality of the *bottom interface*, did not improve. As plasma oxidation time becomes longer than proper oxidation time, values of $V_{+1/2}$ become smaller both before and after annealing [Figs. 5(b)–5(d)]. From this observation, we can conclude that oxidized FM exists at the *bottom interface* in case of over-oxidized tunnel barrier even after annealing so that these defect states become the cause of spin-independent tunneling. It can also be seen that values of $V_{-1/2}$ and their dependence on annealing temperature remain more or less unchanged regardless of different plasma oxidation times, suggesting that the quality of the *top interface* remained unaffected by different plasma oxidation conditions. This result could be ascribed to characteristics of the plasma oxidation, which oxidizes the metallic Al layer after sputtering. Finally, the increase of $V_{\pm 1/2}$ corresponds to the increase in average barrier height $\phi_{1(2)}$, which means that barrier height is also strongly related to the bias-voltage dependence of TMR.

Considering the abovementioned results synthetically, we could conclude that metallic Al layer deposited on epitaxially grown bottom FM layer grows uniformly so that oxygen diffuses into Al layer in order during plasma oxidation. Consequently, the aspect of $V_{\pm 1/2}$ is distinct according to plasma oxidation conditions. In addition, $V_{+1/2}$ is enhanced compared to that of polycrystalline MTJs (~500 mV) fabricated with same plasma oxidation condition due to epitaxially grown bottom FM electrode by which the clean FM electrode-insulator interface with little spin-scattering state is formed.

In summary, expitaxially grown tunnel junctions were fabricated on Al_2O_3 (0001) substrates using UHV sputtering and lithography process. The large values of $V_{\pm 1/2}$ (~650 mV) and barrier height (~3 eV) were obtained after annealing at 250 °C. Furthermore, we could explain the relation between $V_{\pm 1/2}$ and the degree of plasma oxidation based on the qualities of the top and bottom FM layer Al–O layer interfaces.

This study was supported by the IT—program of Research Revolution 2002 (PR2002) “Development of Universal Low-Power Spin Memory” from the Ministry of Education, Culture, Sports, Science and Technology of Japan.

[1] T. Miyazaki and N. Tezuka, J. Magn. Magn. Mater. **139**, L231 (1995).
[2] J. S. Moodera, L. R. Kinder, T. M. Wong, and R. Meservery, Phys. Rev. Lett. **74**, 3273 (1995).
[3] A. H. Davis and J. M. MacLaren, J. Appl. Phys. **87**, 5224 (2000).
[4] X. H. Xiang, T. Zhu, J. Du, G. Landry, and J. Q. Xiao, Phys. Rev. B **66**, 174407 (2002).
[5] J. S. Moodera, J. Nowak, and R. van de Verdonk, Phys. Rev. Lett. **79**, 3744 (1997).
[6] J. Zhang and R. M. White, J. Appl. Phys. **83**, 6512 (1998).
[7] Y. Li, S. X. Wang, G. Khanna, and B. M. Clemens, Thin Solid Films **381**, 160 (2001).
[8] R. F. C. Farrow, G. R. Harp, R. F. Marks, T. A. Rabedeau, M. F. Toney, D. Weller, and S. S. P. Parkin, J. Cryst. Growth **133**, 47 (1993).
[9] W. F. Brinkman, R. C. Dynes, and J. M. Rowell, J. Appl. Phys. **41**, 1915 (1970).
[10] J. Nowak, D. Song, and E. Murdock, J. Appl. Phys. **87**, 5203 (2000).
[11] M. Sato, H. Kikuchi, and K. Kobayashi, IEEE Trans. Magn. **35**, 2946 (1999).
[12] M. F. Gillies, W. Oepts, A. E. T. Kuiper, and R. Coehoorn, IEEE Trans. Magn. **35**, 2991 (1999).
[13] J. J. Sun, K. Shimazawa, N. Kasahara, K. Sato, S. Saruki, T. Kagami, O. Redon, S. Araki, H. Morita, and M. Matsuzaki, Appl. Phys. Lett. **76**, 2424 (2000).
[14] T. Zhu, X. Xiang, and J. Q. Xiao, Appl. Phys. Lett. **82**, 2676 (2003).

Downloaded 11 Jun 2008 to 130.34.135.158. Redistribution subject to AIP license or copyright; see http://apl.aip.org/apl/copyright.jsp